Korean J. Chem. Eng., 40(9), 2209-2218 (2023)
DOI: 10.1007/s11814-023-1395-1

pISSN: 0256-1115
eISSN: 1975-7220

Photoelectrocatalysis performance of Se doped-TiO_2/Ti nanotube arrays for visible-light-driven degradation of diazinon pesticide

Muhammad Nurdin*,,†, Abdul Haris Watoni*, Muhammad Natsir*, Sarifa Rahmatilah*, Maulidiyah Maulidiyah*, Dwiprayogo Wibowo**, La Ode Agus Salim***, Siti Naqiyah Sadikin****, Catherina Manukpadang Bijang*****, and Akrajas Ali Umar******

*Department of Chemistry, Faculty of Mathematics and Natural Sciences, Universitas Halu Oleo, Kendari 93232 - Southeast Sulawesi, Indonesia
**Department of Environmental Engineering, Universitas Muhammadiyah Kendari, Kendari 93127 - Southeast Sulawesi, Indonesia
***Department of Chemistry, Faculty of Science and Technology, Institut Sains Teknologi dan Kesehatan (ISTEK) 'Aisyiyah Kendari, Kendari 93116 - Southeast Sulawesi, Indonesia
****Institute of Microengineering and Nanoelectronics, Universiti Kebangsaan Malaysia, UKM Bangi 43600 - Selangor, Malaysia
*****Department of Chemistry, Faculty of Mathematics and Natural Sciences, Pattimura University, Ambon 97233 - Maluku, Indonesia

(*Received 13 September 2022 • Revised 17 December 2022 • Accepted 31 December 2022*)

Abstract−The modification of ternary metal oxide to improve the photoelectrocatalysis (PEC) properties of TiO_2 photocatalyst is a hot issue in environmental and resource applications. Herein, we present a novel photoelectrocatalytst of Se doped-TiO_2/Ti nanotube arrays (Se@TiO_2/Ti-NTAs) for high-efficiency degradation of diazinon pesticide. The Se@TiO_2/Ti-NTAs were prepared to treat the TiO_2-NTAs in Se-TiO_2 sol-gel for 10 min, which was followed by calcination in air at 200 °C for 1 h. Optical absorption spectroscopy of the Se@TiO_2/Ti-NTAs indicated that there is a redshift in the optical energy gap to 2.95 eV if compared to the pristine TiO_2/Ti NTAs, which suggests that the new photoelectrocatalyst is photoactive under visible light irradiation. We evaluated the photoactivity of the sample by using it as the photoelectrocatalyst in the degradation of diazinon pesticides under the PEC process. The results showed that the Se@TiO_2/Ti-NTAs can degrade 95.62% for 1 h under visible light irradiation, which is equivalent to the degradation rate constant of 0.0183 s^{-1}. For comparison, the pristine TiO_2/Ti NTAs only degrades the diazinon as high as 87.65%, even then under UV light irradiation. Our result also indicated that the Se@TiO_2/Ti-NTAs promote active photoelectron transfer and active radical formation, such as •OH and $•O_2^-$, for rapid diazinon pesticide degradation. The Se@TiO_2/Ti-NTAs photoelectrode should be a potential platform for environmental pollution treatment.

Keywords: Photoelectrocatalysis, Degradation, Pesticide, Diazinon, Se@TiO_2/Ti-NTAs Photoelectrode

INTRODUCTION

The increase in the demand for agricultural products has triggered the use of harmful pesticides in the field [1,2]. The presence of organic pesticides certainly creates a serious problem of environmental pollution due to their toxic nature, which in turn impacts human health [3-5]. This is because the pesticide residues that accumulate in the soil will have an impact on endocrine activity disruption and damage the reproductive and immune systems of living things [1,6].

Today, there are 17 types of pesticides circulating in most South-East Asian countries, particularly Indonesia. Diazinon pesticide is among the most frequently used in this case. Diazinon is an organophosphate insecticide that is widely used in agriculture to control pests on rice, flowers, and vegetables [7,8]. Unfortunately, it is categorized as persistent organic pollutant (POP) because of highly persistent properties in nature, which are difficult to degrade [9,10]. Poisoning by diazinon pesticides causes the body to become weak, suffer convulsions, diarrhea, depression, and death [11]. Therefore, controlling the permissible level of diazinon in the environment and agricultural products is crucial.

There have been several technologies for pesticide residue treatment, including biodegradation [12], adsorption [13], membrane filtration [14], and electrochemical oxidation [5,15]. Though these methods are non-destructive, they only move the garbage to another phase, because it still causes side effects. This creates new problems. In recent years, advanced oxidation techniques have been developed to deal with organic pollutants based on PEC degradation [16,17]. It is a combination method between electrochemical and photocatalysis processes to enhance the degradation of organic pollutants [18,19]. It has been reported that the PEC process can transform organic pollutants into harmless compounds, such as H_2O and CO_2, with more efficient use of chemicals and energy [20,21]. As has been well-known, this process uses a catalyst as a medium to accelerate the oxidation reaction of pesticides. Titanium dioxide

†To whom correspondence should be addressed.
E-mail: mnurdin06@yahoo.com

(TiO_2) is among the semiconductor materials often used for this process due to its high-oxidizing agent, particularly when being irradiated with ultraviolet light (λ 388 nm) [22-25]. Under UV irradiation, the electron at the valence band of the TiO_2 photocatalyst is excited to the conduction band, leaving a hole in the valence band [26-28]. The reaction between excited electrons and water will produce hydroxyl radical (•OH) that in turn attacks organic or pesticide pollutants. Unfortunately, TiO_2 is only active under UV light irradiation because of its relatively high bandgap energy of 3.2 eV [29,30]. This causes the degradation of organic or pesticides to be not economical due to the high-power consumption of UV light during the photocatalytic degradation process. To overcome these limitations, shifting the optical energy band gap of TiO_2 to the visible region is the most chosen alternative for photocatalytic degradation of organics or pesticide contamination under visible light irradiation, which is freely available if using solar irradiation.

There has been a range of approaches to modify the photoactivity of TiO_2 photocatalysts, particularly by metal or non-metal dopings to down-shift the optical energy band gap to the visible region [31-33]. Earlier reports indicated that effective red-shifting of the TiO_2 band gap can be achieved via metal doping, such as platinum (Pt) [34], manganese (Mn) [35], nickel (Ni) [36], molybdenum (Mo) [37,38], and palladium (Pd) [39], and non-metal dopings, such as nitrogen (N) [40], sulfur (S) [41], fluorine (F) [42], and phosphorus (P) [43]. Compositing the TiO_2 with other metaloxide has also been demonstrated to improve the photocatalytic properties in the applications [44,45]. Recently, it has been reported that chalcogenide doping promises a unique photoactivity enhancement in the TiO_2 photocatalyst due to its high stability electropositivity and photoconductivity [46,47]. Selenium, (Se), particularly, has been used to enhance TiO_2 photocatalytic properties in degrading organic pollutants under visible light [48,49]. Owing to its unique photoactivity, exploring the Se-doped TiO_2 in degrading harmful pesticides in the environment should be actively demonstrated to mitigate their unwanted consequences. Here, we report a highly efficient diazonin pesticide degradation over photoelectrocatalyst Se@TiO_2/Ti-NTAs photoelectrode under visible light irradiation. Our results show that the photoelectrode can degrade more than 95% of diazonin within 1 h of reaction under visible light, producing an average kinetic degradation rate as high as 0.0183 $M^{-1}\cdot min^{-1}$. This is doubly higher than the pristine TiO_2/Ti NTAs photoelectrode performance under visible light irradiation. The sample preparation and the performance analysis will be discussed in detail.

MATERIALS AND METHODS

1. Preparation of TiO_2/Ti NTAs

The TiO_2/Ti NTAs were fabricated from a Ti plate via an anodization process, which was adapted from our earlier report [50]. Briefly, the Ti plate (Shanxi Yuanlian Rare Metals Limited, China) was cut to a size of 4.0 cm×0.5 cm and sanded using fine sandpaper (1200CC) until clean and shiny. Subsequently, it was washed using distilled water (di-water) to remove the metal residues and dried at ambient temperature. It was etched using acid solution (HF, (Merck, Germany), HNO_3 (Merck, Germany), and di-water; in a ratio of 1 : 3 : 6 mL, for 2 min to fabricate a hole-tube template and remove oil on the Ti plate surface. Finally, it was rinsed with di-water to remove the remaining etching solution and dried at ambient temperature. The prepared Ti plate was inserted into the probe glass containing an electrolyte solution of 98% glycerol (Merck, Germany) and di-water with a ratio of 9 : 1 and 0.99 g NH_4F (Merck, Germany). The anodization was conducted by placing the Ti plate as the anode, and the Cu plate as the cathode and biased with 25 Volts DC for 4 h. The sample was then calcined for 1.5 h at 500 °C.

2. Preparation of Se-doped TiO_2/Ti-NTAs

Se doped TiO_2/Ti NTAs (Se@TiO_2/Ti-NTAs) was prepared by dip-coating of pristine TiO_2/Ti NTAs into a Se sol-gel. Prior to the Se doping process, the Se sol-gel was first prepared by mixing 0.43 g of selenonic acid (98.1%) with 15.0 mL of ethylene glycol ($C_2H_6O_2$). We called this Solution A. At the same time, another solution (solution B) was prepared by dissolving 4.0 mL of titanium tetraisopropoxide (TTIP 97%) in 15.0 mL of ethylene glycol. Solutions A and B were then mixed and refluxed for 10 h at 60 °C until a white color solution was produced. The sample was heated to evaporate the solvent at 80 °C for 1 h. This finally produced a Se-TiO_2 sol-gel. The pristine TiO_2/Ti NTAs were then immersed into the Se-TiO_2 sol-gel 10 min. The sample was finally calcined for 15 min at 200 °C to obtain the Se@TiO_2/Ti-NTAs photoelectrode.

3. Characterization

The TiO_2/Ti-NTAs photoelectrode was characterized using X-ray diffraction (XRD) to obtain information on the crystallinity properties of the sample. The morphology of the sample was analyzed using field-emission scanning electron microscopy (FESEM) technique by JEOL JIB-4610F Multi Beam System field-emission electron microscopy apparatus), which was equipped with electron-energy diffraction spectroscopy (EDX) for elemental analysis of the samples. Optical properties were determined using an ultraviolet-visible diffuse reflectance spectrophotometer (UV-Vis DRS). The optical band gap of the sample was evaluated from the reflectance spectrum using the Kubelka-Munk equation. Finally, the PEC current was evaluated using linear sweep voltammetry (LSV) to obtain the nature of electron transfer in the material.

4. Photoelectrocatalysis Experiments

Photoelectrocatalytic properties of the samples were evaluated in the degradation of diazinon pesticide under visible light irradiation. The measurement was carried out using the multi-pulse amperometry (MPA) technique. In the typical PEC process, diazinon pesticide of concentration of 0.5 $mg\cdot L^{-1}$; 1.0 $mg\cdot L^{-1}$; 2.0 $mg\cdot L^{-1}$, and 3.0 $mg\cdot L^{-1}$ in 0.1 M $NaNO_3$ electrolyte solution were analyzed. The reaction duration was 10 min under a bias potential of 0.5 Volts DC. The photoelectrocatalytic properties of the sample under UV and visible light irradiation were evaluated. The UV light source with a wavelength of 360 nm was from a Mercury lamp with a power of 15 Watts. Meanwhile, visible light from the xenon lamp had a power of 18 Watts. The diazinon pesticide degradation was determined by measuring the optical absorbance of diazinon every 10 min in 1 h observation.

RESULTS AND DISCUSSION

1. TiO_2/Ti-NTAs and Se@TiO_2/Ti-NTAs Photoelectrodes

The TiO_2/Ti NTAs and Se@TiO_2/Ti NTAs were obtained from the anodization process of Ti plate [50]. The following equations describe how the reaction progresses and the nanostructures forms:

Oxidation on Ti Plate: $Ti \rightarrow Ti^{4+} + 4e^-$ (1)

Water splitting: $2H_2O \rightarrow 2O^{2-} + 4H^+$ (2)

Formation of oxide layer: $Ti^{4+} + 2O^{2-} \rightarrow TiO_2$ (3)

Formation of nanotubes: $TiO_2 + 6F^- + 4H^+ \rightarrow [TiF_6]^{2-} + 2H_2O$ (4)

Eqs. (1) and (2) show the oxidation reaction of Ti to Ti^{4+} that releases four electrons (Eq. (1)), and the water-splitting reaction that produces $2O_2^-$ and $4H^+$ (Eq. (2)). These conditions promote the unique reactions between Ti^{4+} and $2O_2^-$ to form amorphous TiO_2. The nanotubes arrays (NTAs) were formed via the reaction of TiO_2 and ionized $6NH_4F$ ($6F^- + 6NH_4^+$) and $4H^+$ (water splitting) that produces $[TiF_6]^{2-}$ and water. The presence of $[TiF_6]^{2-}$ on the Ti surface is the key factor for NTAs formation [51,52]. With the calcination process, crystalline TiO_2 NTAs on Ti plate is then realized. In general, the anodizing process will create nanomaterials that have sizes between 1-500 nm [53,54]. In this study, the glycerol as a supporting electrolyte may have reduced current fluctuation and resulted in a softer nanotube wall. Nanotubes or porous TiO_2 photocatalyst is aimed to form a large surface area that can be used as sites for the photocatalysis process in degrading organic compounds. However, the Se-doped TiO_2/Ti NTAs formation used the as-prepared amorphous TiO_2 to promote Se metal ion attachment during immersion in Se-TiO_2 sol-gel. This method is simple for growing nanoparticles and relatively inexpensive, where the substrate is immersed in a core solution (precursor). Se ions are expected to trigger a dual effect that can improve the performance of TiO_2. The first effect is a decrease in the TiO_2 energy bandgap due to the overlap of the titanium 3d orbitals with the 4p Se orbitals, which causes new electron energy levels below the conduction band. The second effect is the inhibition of electron recombination while prolonging the lifetime of the electron-hole pair. In some photocatalytic reaction processes, the lifetimes of electrons and holes should be extended so that these species can move to the surface of the semiconductor [55]. The addition of Se ions as a dopant triggers the formation of a new trapping site that functions to capture electrons. On the other side, it also has a role in hole trappers to reduce the bandgap value. Fig. 1 illustrates the reduction of the TiO_2 bandgap by Se^{4+} ions.

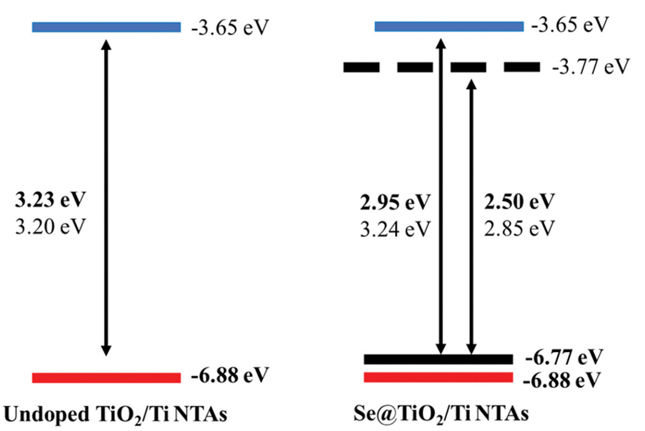

Fig. 1. The energy level diagrams of the undoped and Se@TiO_2/Ti-NTAs adopted from Gurkan et al. [55].

2. Crystallinity and Morphology

Fig. 2(a) shows the XRD diffractogram of undoped photoelectrode that shows the presence of both anatase and rutile phases. For example, the anatase phase is judged from the obtained peaks at 2θ of 25.14 (101); 35.84 (103); 37.83 (004); 47.72 (200); 52.77 (105); 54.83 (211); 62.75 (204), and 68.81 (116), which agree with the COD data No. 96-900-8217; 96-152-8779; and 96-100-8051. This is also in good agreement with the reported results [56-58]. Meanwhile, the rutile phase is indicated by three peaks at 2θ of 41.3 (111); 44.4 (210), and 64.2 (310), which agree with JCPDS 21-1276 [59]. This remarks that the nanotube sample is TiO_2 with mixed-phase crystallinity. However, because the XRD pattern of the Se-doped sample is exactly similar to the undoped one due to the limited resolution of the instrument, we carried out Raman analysis to verify the effect of Se doping on the phase crystallinity of the TiO_2 sample. The result is shown in Fig. 2(b). For the anatase phase with tetragonal symmetry, the spectra contain at least five active Raman characters related to the TiO_2 system, particularly the $1A_{1g}$, $2B_{1g}$,

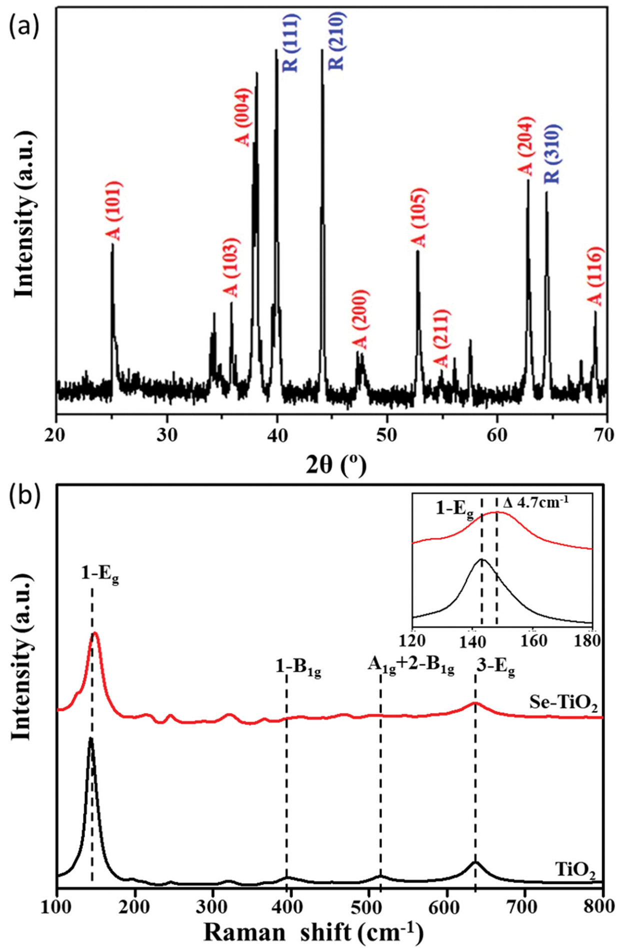

Fig. 2. (a) XRD pattern of undoped (TiO_2/Ti NTAs). (b) Raman shift spectrum for TiO_2 and Se@TiO_2 sample. Inset in b is the zoom-in image at 100 to 200 cm^{-1} region of the Raman spectrum.

and $3E_g$ optical phonon modes. For rutile with orthorhombic symmetry, the active Raman are B_{1g}, E_g, A_{1g}, and B_{2g}. Considering the XRD result presented above, the dominant phase is anatase. Therefore, comparing the active Raman for anatase to verify the doping effect is sufficient. As the result reveals, five active Raman for the anatase phase are obtained, namely $1E_g$ at 143.5 cm^{-1}, $2B_{1g}$ at 396.0 and 513.8 cm^{-1}, A_{1g} at 513.8 cm^{-1}, and $3E_g$ at 636 cm^{-1}. The presence of Se in the TiO_2 lattice causes shifting in the main Eg Raman character as high as 4.7 cm^{-1}, i.e., changes from 143.5 to 148.2 cm^{-1} (inset Fig. 2(b)). The shifting in the Raman mode is certainly due to the distortion of the lattice in the presence of foreign ions. Thus, this confirms the successful doping of the TiO_2 with Se ion.

Fig. 3(a)-(b) present the morphology of both photoelectrodes obtained from the scanning electron microscopy analysis (SEM). The surface morphology of undoped and Se@TiO_2/Ti-NTAs photoelectrodes is completely different where the undoped sample features an irregular honeycomb arrangement of nanotubes with an average tube diameter of approximately 500 nm. In contrast, the Se@TiO_2/Ti-NTAs that were produced from the sol-gel coating process on TiO_2/Ti-NTAs showed that it consists of much larger particles with an average size of about 100 nm; the result of the Se^{4+} ions doping involved in the TiO_2/Ti-NTAs causes a fine agglomeration of the sol-gel material. In addition, the tendency of agglomeration can also be attributed to the fact that doping of impurities leads to the formation of new defects, calcination effects, and dislocations in the crystal lattice. The elemental compositions on the

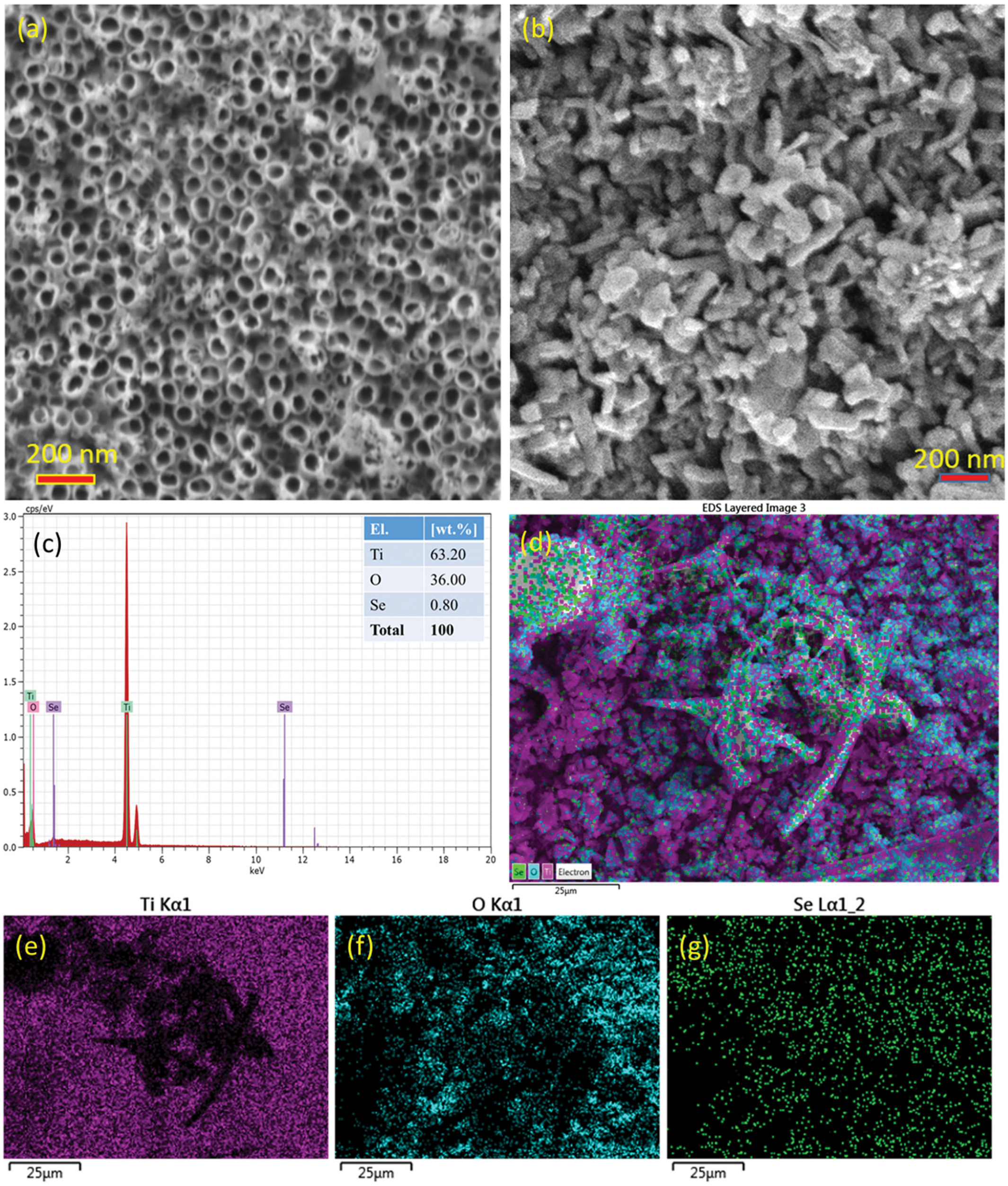

Fig. 3. The micrograph and elemental identification. (a) FESEM image of TiO_2/Ti NTAs and (b) Se@TiO_2/Ti-NTAs photoelectrodes. (c) EDX spectrum for Se@TiO_2/Ti-NTAs. (d)-(g) elemental mapping for Se@TiO_2/Ti-NTAs sample.

Se@TiO_2/Ti-NTAs photoelectrode were identified using EDX to confirm the presence of Se onto TiO_2/Ti-NTAs. It is shown that three elements, i.e., Ti (0.4 KeV and 4.5 KeV), Se (1.4 KeV and 11.2 KeV), and O (0.5 KeV) were observed from the spectrum. This certainly confirms the formation of Se@TiO_2/Ti-NTAs. The EDX elemental mapping (Fig. 3(d)-(g)) further shows the nature of elemental distribution in the sample, where the Se is homogeneously distributed in the sample.

The chemical state of the Se dopant certainly determines the properties of the TiO_2 system. Considering the large ionic radius of the Se if compared with the O ion, the substitution of O by the Se site is unlikely. Therefore, as mentioned above, the Se should be in 4+ oxidation state to substitute any Ti^{4+} vacancy in the lattice, which has been reported elsewhere in the literature.

The formation of nanotubes is mainly caused by two effects of the fluoride ions: (i) the ability to form water-soluble ($[TiF_6]^{2-}$) complexes, and (ii) the small ionic radius that makes them suitable to penetrate through the growing TiO_2 lattice and thus competing with O_2^- transport. The complex formation ability leads to a continuous chemical dissolution of formed TiO_2. The current response of the process under applied potential represents three stages of the process: (i) the growth of compact TiO_2 occurs. (ii) The initial stage of the formation of the nanotubes. In the second stage, the fluoride ions interact with TiO_2, and selective dissolution in the high-energy facet. The increasing current is a consequence of competition between oxidation (electrochemical process) and chemical dissolution of the oxide layer. (iii) The equilibrium between oxidation and dissolution is reached. At this stage, the current flow is constant, reflecting the formation of nanotubes [60].

3. Optical Absorption and Photoelectrochemical Response

Fig. 4(a) shows UV-visible diffuse reflectance (UV-DRS) spectra for the undoped and Se@TiO_2/Ti-NTAs. By using the reflectance spectra and the Kubelka-Munk formula [61],

$$F(R)=\frac{(1-R)^2}{2R} \tag{5}$$

where R is the reflectance read from the spectrum, along with the Tauc equation for plotting $[F(R).\ h\upsilon]^n$ vs $h\upsilon$, where $h\upsilon$ is the photon energy and n=½, the energy band edge of the sample can be estimated (Fig. 2(b)). As the figure reveals, the spectrum for the pristine sample has a sharp energy edge at around 3.23 eV, whereas the Se@TiO_2/Ti-NTAs has an energy absorption edge at 2.95 eV. These results reflect that the Se@TiO_2/Ti-NTAs should have photoactivity in the visible light region. Meanwhile, the pristine sample is active under UV light. Gurcan et al. [55] reported that high concentrations of Se^{4+} ions doped into the TiO_2 can reduce the bandgap energy for effective photodegradation of 4-Nitrophenol (4-NP) compound. In addition, lower bandgap energy of Se@TiO_2/Ti-NTAs may reduce the energy needed to excite electrons and increase the opportunity for charge carriers to reach the photoelectrocatalyst surface.

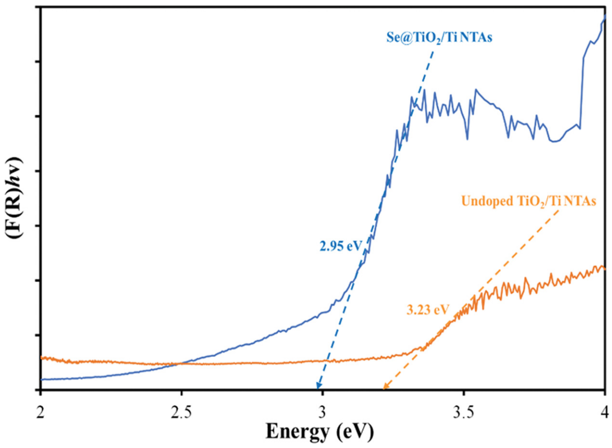

Fig. 4. UV-DRS spectra of the undoped and Se@TiO_2/Ti-NTAs (orange: TiO_2/Ti-NTAs; blue: Se@TiO_2/Ti-NTAs).

The optical properties of both photoelectrodes also have a relationship with the photocurrent response under the photoelectrochemical process. When the photoelectrode is exposed to UV or visible light, it responds by exciting electrons to the excited state, in which the excited level is proportional to the light energy transmitted to the photoelectrode in the photoelectrochemical process. This process can be observed by the linear sweep voltammetry (LSV) method [62].

The photoelectrodes (undoped and Se@TiO_2/Ti-NTAs) were placed as a working electrode, platinum (Pt) wire as a counter electrode, and Ag/AgCl electrode as a comparison electrode. The pho-

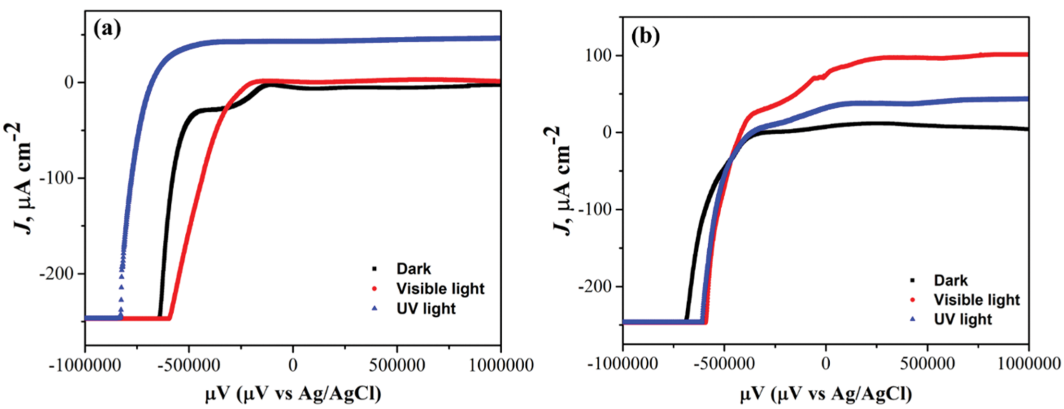

Fig. 5. Photocurrent response of photoelectrodes; (a) undoped (TiO_2/Ti-NTAs), and (b) Se@TiO_2/Ti-NTAs.

toelectrocatalytic properties of the electrode were observed by irradiating the system using UV or visible light during the photoelectrochemical measurement.

Fig. 5 shows the photoelectrochemical responses of the electrodes in dark and the illumination of UV and visible light sources. For the case of the undoped sample, a high photocurrent response was observed under UV light exposure. Meanwhile, under visible light irradiation, the undoped sample is not photoactive so the photocurrent is similar to the one under dark. This certainly fits the optical band gap of the undoped sample, which is at the UV energy region (3.23 eV), so it requires a large amount of energy to activate the movement of electrons on the surface of the electrode to initiate a redox reaction in the PEC process. For the Se@TiO_2/Ti-NTAs sample, the highest photocurrent was obtained when the electrode was irradiated by the visible light source. The photocurrent significantly exceeds the one under UV light irradiation. This is the result of the Se@TiO_2/Ti-NTAs only needing lower light energy to trigger electron excitation in photoelectrode. The addition of Se^{4+} ions decreased the bandgap energy of undoped and acted as an electron acceptor to increase the electron movement on the TiO_2 surface for initiating the PEC reaction. The presence of e^- and h^+ on the semiconductor surface will initiate the high PEC degradation over organic pollutants based on a redox effect on both electrodes (working electrode and counter electrode) [18].

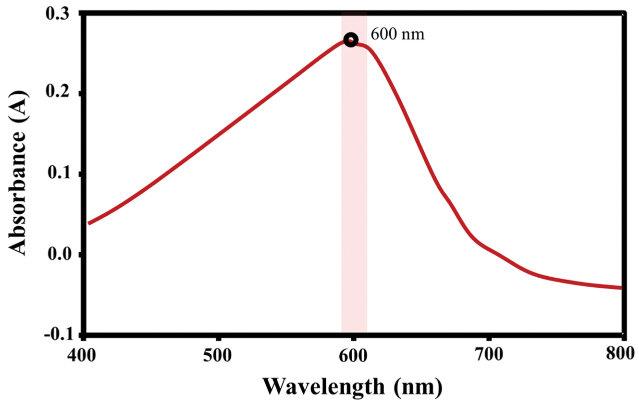

Fig. 6. The maximum wavelength of diazinon pesticide analyzed via UV-Vis spectrophotometer.

4. Degradation Performance

Before the evaluation of the photoelectrocatalytic properties of the electrode, to obtain a change in the concentration of diazinon during the photoelectrocatalytic reaction, we determined the optical absorption spectrum of diazinon pesticide (Fig. 6) using a UV-Vis spectrophotometer and evaluating the relationship between the diazinon concentration and its absorption peak intensity. We

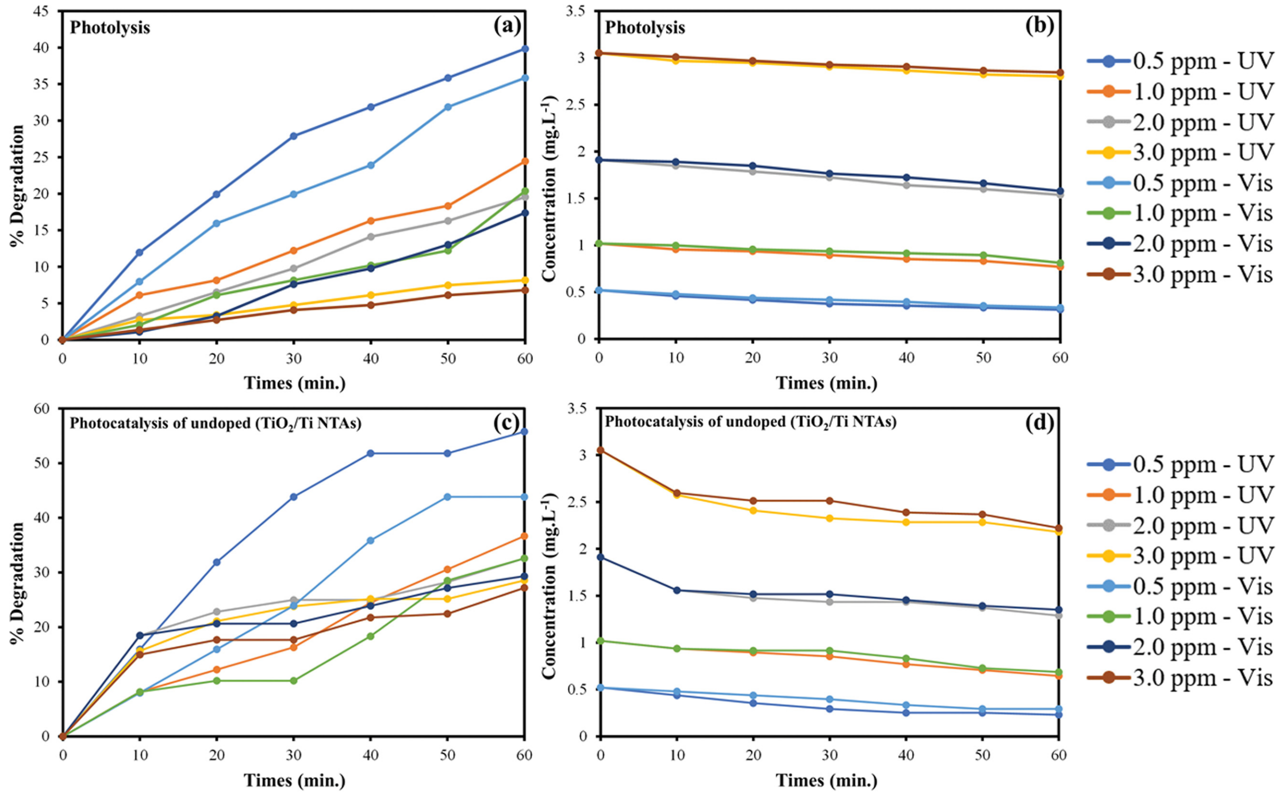

Fig. 7. The graph of degradation test by varying concentrations and photoelectrodes; (a) % degradation of PL; (b) PL test (decrease in concentrations); (c) % degradation of undoped PC; (d) PC test of undoped (decrease in concentrations); (e) % degradation of Se@ TiO_2/Ti-NTAs PC; (f) PC test of Se@TiO_2/Ti-NTAs (decrease in concentrations); (g) % degradation of undoped PEC; (h) PEC test of undoped (decrease in concentrations); (i) % degradation of Se@TiO_2/Ti-NTAs PEC; (j) PEC test of Se@TiO_2/Ti NTAs (decrease in concentrations).

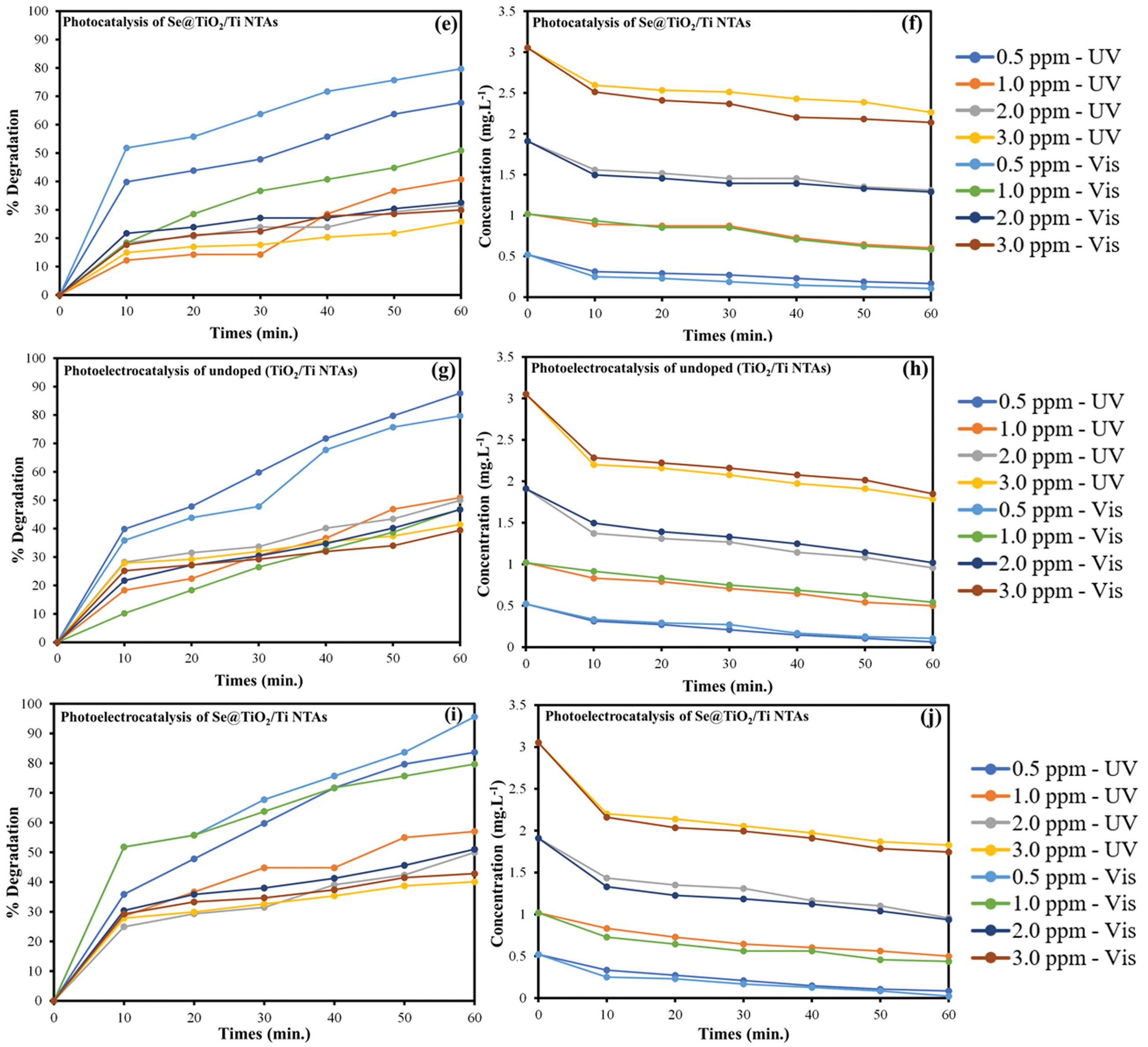

Fig. 7. Continued.

call this a concentration calibration curve. The diazinon has an absorption band centered at 600 nm, which is π electron excitation in the molecules [63]. By using diazinon concentrations of 0.5 $mg \cdot L^{-1}$, 1.0 $mg \cdot L^{-1}$, 2.0 $mg \cdot L^{-1}$, and 3.0 $mg \cdot L^{-1}$, a calibration curve of absorption intensity versus concentration is plotted that obeys the equation of $y=0.0482x+0.0739$. Using this equation, we can determine the concentration of diazinon during the reaction from the intensity of the absorption peak obtained from the UV-vis spectroscopy.

Fig. 7(a)-7(j) is the graph of diazinon pesticide degradation under photolysis, photocatalysis, and photoelectrocatalysis processes. Photolysis is the degradation property of diazinon under UV light irradiation in the absence of a photocatalyst. The rest of the processes are in the presence of a photocatalyst. We evaluated the degradation kinetics of the diazinon using several initial diazinon concentrations to obtain its degradation behavior at a particular concentration. For the photolysis (PL) effect under UV light, the decomposition of diazinon was significantly low for all concentrations. No decomposition was observed under visible light irradiation. This condition is expected as this is required to validate the effect of photocatalysts in the degradation of diazinon in the photoelectrocatalytic process. In contrast, the degradation under photocatalytic effect shows a significant decrease in the diazinon concentration both in the presence of undoped (under UV light) and Se@TiO_2/Ti NTAs (under visible light) photoelectrodes.

Explicitly, the undoped photoelectrode gave a PC response under UV light (0.5 ppm=67.73%; see Table 1), while the visible light did not show good performance. Refer to bandgap spectra (Fig. 2) that the TiO_2/Ti-NTAs has a bandgap of 3.23 eV, which indicates it needed high energy exposure from UV light to excite an electron to initiate a redox reaction, whereas the visible light cannot move electrons to be excited to the conduction band. On the other hand, Se@TiO_2/Ti-NTAs under the influence of visible light in the PC

Table 1. The percentage of degradation tested by varying concentrations and photoelectrodes

Concentrations ($mg\cdot L^{-1}$)	PL (%)		PC undoped (TiO_2/Ti NTAs) (%)		PC Se@TiO_2/ Ti NTAs (%)		PEC undoped (TiO_2/Ti NTAs) (%)		PEC Se@TiO_2/ Ti NTAs (%)	
	UV	Vis	UV	Vis	UV	Vis	UV	Vis	UV	Vis
0.5	39.83	35.86	55.78	43.81	67.73	79.67	87.65	79.67	83.63	95.62
1.0	24.42	20.37	36.66	32.59	40.72	42.77	50.92	46.83	50.92	57.00
2.0	19.53	17.36	32.56	29.32	31.49	32.56	49.95	46.69	49.95	51.02
3.0	8.16	6.80	28.54	27.20	25.81	28.54	41.47	39.43	40.11	42.83

Table 2. The kinetic rate constant (k) under the PEC process for the both photoelectrodes

Concentrations ($mg\cdot L^{-1}$)	k PEC of undoped (TiO_2/Ti NTAs)		k PEC of Se@TiO_2/Ti NTAs	
	UV ($M^{-1}\cdot min^{-1}$)	Vis ($M^{-1}\cdot min^{-1}$)	UV ($M^{-1}\cdot min^{-1}$)	Vis ($M^{-1}\cdot min^{-1}$)
0.5	0.0323	0.0026	0.0298	0.0434
1.0	0.0114	0.0102	0.0111	0.0128
2.0	0.0096	0.0091	0.0098	0.0097
3.0	0.0071	0.0065	0.0069	0.0076
Average ($\bar{x}$)	0.0151	0.0071	0.0144	0.0183
Standard Deviation (SD)	0.0116	0.0033	0.0104	0.0168

process gave a good performance over 0.5 $mg\cdot L^{-1}$ with a degradation percentage of 79.67% (Table 1).

Particularly, the PEC process in both photoelectrodes showed good performance of enhanced PC response, in which the undoped performance had good activity under UV light irradiation, whereas Se@TiO_2/Ti-NTAs gave good performance under visible light irradiation. Uniquely, their performance is higher when compared to PC and PEC processes. It is due to the introduction of low potential difference induction into the PEC process to drive excited electrons from the semiconductor to be transferred to the reference electrode to initiate high-performance degradation of organic compounds. If we pair PC and PEC performance against both photoelectrodes under 0.5 ppm concentration exhibiting that undoped has a percentage degradation value of 55.78% and 87.65% under UV irradiation, while Se@TiO_2/Ti-NTAs have a percentage degradation value of 79.67% and 95.62%, respectively (Table 1). This performance is impressively higher than the recently reported results, such as using N-TiO_2/graphene/Au or N-TiO_2/graphene/Ag electrodes [64], N-TiO_2/Ag/Ti [65], WO_3 nanostructures film electrode [66]. Unfortunately, when the concentration of diazinon pesticide is increased, the performance of both photoelectrodes decreases because higher sample concentrations will impact the closure of the active site on the photoelectrodes surface so that the degradation performance slows. In addition, this condition also makes it difficult for light energy exposure to penetrate photoelectrodes [67,68]. Consequently, the PC and PEC processes can be applied by expanding the surface area and using an aerator to reduce of saturation level on the photoelectrodes surface.

Table 2 is the kinetic rate constant (k) under the PEC process for both photoelectrodes. It shows the determination of k based on the Langmuir-Hinshelwood formula followed by the first order, where the determination of k has been applied by plotting ln C_0/C_t divided by time. Uniquely with high sample concentrations occurring, the value of k decreases [69,70]. It is due to the high concentrations that have covered the active sites on both photoelectrodes; theoretically, the active sites should be proportional to the high sample concentrations. Consequently, the low concentrations are easily absorbed on photoelectrodes to initiate high-degradation under the PEC process. Based on the data, Table 2 shows that the performance of the both photoelectrodes are at close intervals; the only difference is seen from its degradation performance when irradiated under UV light for undoped and visible light for Se@TiO_2/Ti-NTAs.

As mentioned, the degradation of diazinon was judged from the decrease of the characteristic optical absorption peaks of diazinon, particularly at 600 nm. In the typical process, the degradation of diazinon under the photoelectrocatalysis process produces small molecules of diazoxon and 2-isopropyl-6-methyl-pyrimidin-4-ol (IMP). However, the product would be depending on the condition of the reaction, particularly the type of catalyst. Certainly, the analysis of the product, such as using mass spectrometry, would be critical for correlating the condition of the reaction with the product. Nevertheless, because the present study evaluated the Se doping of the TiO_2 photocatalyst on the photoelectrocatalytic degradation of diazinon, the change in the concentration of the diazinon is sufficient. However, evaluating how the photocatalyst properties influence the product is interesting. Thus, we are pursuing the analysis and will report the result differently.

CONCLUSION

In this work, higher-order undoped (TiO_2/Ti-NTAs) and Se@TiO_2/Ti-NTAs photoelectrodes were fabricated using a combination of anodization and sol-gel methods and their application to degrade diazinon pesticide under the PEC process. We report that the dip-coating technique for coating TiO_2/Ti NTAs using Se^{4+} ions was very effective in degrading diazinon pesticides under PC and PEC processes. In addition, the variation of light exposure (UV and visible lights) on both photoelectrodes effectively degraded samples in both processes. However, the PEC process had a dominant good performance compared to the PL and PC processes. It is due to the inducted potential charge from potentiostat to the working electrode having given high-redox reaction in the PEC process. Both photoelectrodes showed good performance under low concentrations caused by presenting of active sites and high surface area on both photoelectrodes.

ACKNOWLEDGEMENT

We acknowledge the financial support from the Ministry of Education, Culture, Research and Technology of the Republic of Indonesia under the World Class Professor award grant no. 3252/E4/DT.04.03/2022.

REFERENCES

1. M. Zeshan, I. A. Bhatti, M. Mohsin, M. Iqbal, N. Amjed, J. Nisar, N. AlMasoud and T. S. Alomar, *Chemosphere*, **300**, 134525 (2022).
2. A. K. Paul, S. K. Mukherjee and S. T. Hossain, *Dev. Wastewater Treat. Res. Process.*, 515 (2022).
3. A. Saravanan, P. S. Kumar, S. Jeevanantham, M. Anubha and S. Jayashree, *Environ. Pollut.*, **298**, 118844 (2022).
4. A. Intisar, A. Ramzan, T. Sawaira, A. Kareem, N. Hussain, M. I. Din, M. Bilal and H. M. N. Iqbal, *Chemosphere*, **293**, 133538 (2022).
5. T. Azis, M. Maulidiyah, M. Z. Muzakkar, R. Ratna, S. W. Aziza, C. M. Bijang, O. A. Prabowo, D. Wibowo and M. Nurdin, *Surf. Eng. Appl. Electrochem.*, **57**, 387 (2021).
6. X. Fu, R. Yang, G. Zhou, X. Chen, Y. Liu, J. Chi, X. Li, H. Fang, H. Li and W. Li, *Curr. Opin. Green Sustain. Chem.*, 100629 (2022).
7. F. Barjasteh-Askari, S. Nasseri, R. Nabizadeh, A. Najafpoor, M. Davoudi and A.-H. Mahvi, *Environ. Sci. Pollut. Res.*, **29**, 26113 (2022).
8. S. D. Lesmana, E. Maryanti, E. Susanty, D. Afandi, W. Harmas, D. N. Octaviani, I. Zulkarnain, M. A. B. Pratama and M. Mislindawati, *Reports Biochem. Mol. Biol.*, **10**, 589 (2022).
9. J. O. Ighalo, P.-S. Yap, K. O. Iwuozor, C. O. Aniagor, T. Liu, K. Dulta, F. U. Iwuchukwu and S. Rangabhashiyam, *Environ. Res.*, **212**, 113123 (2022).
10. L. Fei, M. Bilal, S. A. Qamar, H. M. Imran, A. Riasat, M. Jahangeer, M. Ghafoor, N. Ali and H. M. N. Iqbal, *Environ. Res.*, **211**, 113060 (2022).
11. R. Zia, A. Taj, S. Younis, S. Z. Bukhari, F. Latif, Y. Feroz, K. Fatima, A. Imran and S. Z. Bajwa, in *Nanosensors smart agric.*, Elsevier, 259 (2022).
12. T. Ebadi, G. D. Najafpour, H. Younesi and M. Mohammadi, *Environ. Technol. Innov.*, **25**, 102218 (2022).
13. Maulidiyah, D. Wibowo, Hikmawati, R. Salamba and M. Nurdin, *Orient. J. Chem.*, **31**, 2337 (2015).
14. S.-E. Ban, E.-J. Lee, D.-J. Lim, I.-S. Kim and J.-W. Lee, *Bioresour. Technol.*, **348**, 126828 (2022).
15. M. Nurdin, M. Maulidiyah, A. H. Watoni, A. Armawansa, L. O. A. Salim, Z. Arham, D. Wibowo, I. Irwan and A. A. Umar, *Korean J. Chem. Eng.*, **39**, 209 (2022).
16. D. Wibowo, Maulidiyah, Ruslan, T. Azis and M. Nurdin, *Anal. Bioanal. Electrochem.*, **10** (2018).
17. M. Nurdin, D. Wibowo, M. Natsir, H. Ritonga and A. H. Watoni, *Int. J. ChemTech Res.*, **8**, 416 (2015).
18. M. Nurdin, D. Wibowo and A. Sani, *Int. J. Pharm. Pharm. Sci.*, **7**, 141 (2015).
19. M. Nurdin, T. Azis, M. Maulidiyah, A. Aladin, N. A. Hafid, L. O. A. Salim and D. Wibowo, *IOP Conf. Ser. Mater. Sci. Eng.*, **367**, 012048 (2018).
20. Y. Zhang, X. Xiong, Y. Han, X. Zhang, F. Shen, S. Deng, H. Xiao, X. Yang, G. Yang and H. Peng, *Chemosphere*, **88**, 145 (2012).
21. M.-Z. Ge, C.-Y. Cao, J.-Y. Huang, S.-H. Li, S.-N. Zhang, S. Deng, Q.-S. Li, K.-Q. Zhang and Y.-K. Lai, *Nanotechnol. Rev.*, **5**, 75 (2016).
22. M. Nurdin, N. Dali, I. Irwan, M. Maulidiyah, Z. Arham, R. Ruslan, B. Hamzah, S. Sarjuna and D. Wibowo, *Anal. Bioanal. Electrochem.*, **10**, 1538 (2018).
23. M. Z. Muzakkar, M. Nurdin, I. Ismail, M. Maulidiyah, D. Wibowo, R. Ratna, S. K. M. Saad and A. A. Umar, *Emiss. Control Sci. Technol.*, **6**, 28 (2020).
24. D. Wibowo, Y. Sufandy, I. Irwan, T. Azis, M. Maulidiyah and M. Nurdin, *J. Mater. Sci. Mater. Electron.*, **31**, 14375 (2020).
25. M. Natsir, M. Maulidiyah, A. H. Watoni, J. Arif, A. Sari, L. O. A. Salim, S. Sarjuna, I. Irwan and M. Nurdin, *J. Phys. Conf. Ser.*, **1899**, 012039 (2021).
26. M. Natsir, Y. I. Putri, D. Wibowo, M. Maulidiyah, T. Azis, C. M. Bijang, F. Mustapa, I. Irwan, Z. Arham and M. Nurdin, *J. Inorg. Organomet. Polym. Mater.*, **31**, 3378 (2021).
27. D. Wibowo, R. H. A. Malik, F. Mustapa, T. Nakai, M. Maulidiyah and M. Nurdin, *J. Oleo Sci.*, **71**, 759 (2022).
28. M. Z. Muzakkar, M. Natsir, A. Alisa, M. Maulidiyah, L. O. A. Salim, I. Sulistiyani, F. Mustapa, Ratna and M. Nurdin, *J. Phys. Conf. Ser.*, **1899**, 012043 (2021).
29. M. Nurdin, N. A. Yanti, Suciani, A. H. Watoni, Maulidiyah, A. Aladin and D. Wibowo, *Asian J. Chem.*, **30**, 1378 (2018).
30. D. Wibowo, W. O. S. I. Sari, A. Said, F. Mustapa, B. Susianti, M. Maulidiyah and M. Nurdin, *Anal. Bioanal. Electrochem.*, **14**, 385 (2022).
31. D. Wibowo, Ruslan, Maulidiyah and M. Nurdin, *IOP Conf. Ser. Mater. Sci. Eng.*, **267**, 012007 (2017).
32. L. O. Mursalim, A. M. Ruslan, R. A. Safitri, T. Azis, Maulidiyah, D. Wibowo and M. Nurdin, in *IOP Conf. Ser. Mater. Sci. Eng.* (2017).
33. M. Maulidiyah, E. Widianingsih, T. Azis and D. Wibowo, *ARPN J. Eng. Appl. Sci.*, **10**, 6250 (2015).
34. S. B. Potdar, C. M. Huang, B. Praveen, S. Manickam and S. H. Sonawane, *Catalysts*, **12**, 78 (2022).
35. M. Maulidiyah, P. E. Susilowati, N. K. Mudhafar, Z. Arham and M. Nurdin, Biointerfaceresearch.com (2021).
36. R. Senthamarai, V. Madurai Ramakrishnan, P. Murugan, A. Ponnusamy Munusamy and S. Kulandhaivel, *Int. J. Energy Res.*, **46**, 7749 (2022).
37. S. Kader, M. R. Al-Mamun, M. B. K. Suhan, S. B. Shuchi and M. S. Islam, *Environ. Technol. Innov.*, **27**, 102476 (2022).
38. T. Wang, X. Lang, L. Li, C. Yao, R. Shi and K. Cai, *Int. J. Energy Res.*, **46**, 5342 (2022).
39. G. O. Obaiah, K. H. Shivaprasad, S. K. Bhat and M. Mylarappa,

ECS Trans., **107**, 1681 (2022).
40. Maulidiyah, T. Azis, A. T. Nurwahidah, D. Wibowo and M. Nurdin, *Environ. Nanotechnol., Monit. Manag.*, **8**, 103 (2017).
41. Y. Wang, L. Yin, J. Wu, N. Li, N. He, H. Zhao, X. Li, X. Lai and Q. Wu, *J. Mater. Sci.*, 1 (2022).
42. W. Diao, J. Xu, X. Rao and Y. Zhang, *Catal. Lett.*, **152**, 1029 (2022).
43. D. R. Sarker, M. N. Uddin, M. Elias, Z. Rahman, R. K. Paul, I. A. Siddiquey, M. A. Hasnat, M. R. Karim, M. A. Arafath and J. Uddin, *Clean. Eng. Technol.*, **6**, 100364 (2022).
44. Y. Wang, J. Li, B. Wang, M. Sun, X. Yan, L. Chen, G. Bai and Y. Li, *New J. Chem.*, **45**, 6247 (2021).
45. J. Li, B. Wang, Y. Pang, M. Sun, S. Liu, W. Fang and L. Chen, *Colloids Surf. Physicochem. Eng. Aspects*, **638**, 128297 (2022).
46. S. Nivetha, R. Perumalsamy, A. Ayeshamariam, M. P. Srinivasan, and A. Mohamed Saleem, *Fluid Mech. Open Acc.*, **4**, 2296 (2017).
47. P. Srathongluan, R. Kuhamaneechot, P. Sukthao, V. Vailikhit, S. Choopun and A. Tubtimtae, *J. Colloid Interface Sci.*, **463**, 222 (2016).
48. W. Song, C. Ma, S. Yan, R. Shi, L. Zhang, T. Gao, B. Li, N. Chen and Z. Qiu, *Scr. Mater.*, **215**, 114705 (2022).
49. H. Xu, D. Liu, W. Wang and G. Yu, *Inorg. Chem.*, **61**, 3121 (2022).
50. M. Nurdin, D. Wibowo, T. Azis and R. Ayu, *Surf. Eng. Appl. Electrochem.*, **58**, 125 (2022).
51. Nurhidayani, M. Z. Muzakkar, Maulidiyah, D. Wibowo and M. Nurdin, *IOP Conf. Ser. Mater. Sci. Eng.*, **267**, 012035 (2017).
52. D. Wibowo, M. Z. Muzakkar, M. Maulidiyah, M. Nurdin, S. K. M. Saad and A. A. Umar, *Biointerface Res. Appl. Chem.*, **12**, 1421 (2021).
53. A. G. Munoz, *Electrochim. Acta*, **52**, 4167 (2007).
54. J. Park, S. Bauer, A. Pittrof, M. S. Killian, P. Schmuki and K. von der Mark, *Small*, **8**, 98 (2012).
55. Y. Y. Gurkan, E. Kasapbasi and Z. Cinar, *Chem. Eng. J.*, **214**, 34 (2013).
56. J. Wang, J. Yu, X. Zhu and X. Z. Kong, *Nanoscale Res. Lett.*, **7**, 1 (2012).
57. S. Noothongkaew, H. K. Jung, O. Thumtan and K.-S. An, *Mater. Lett.*, **233**, 153 (2018).
58. S. Noothongkaew, O. Thumthan and K.-S. An, *Mater. Lett.*, **218**, 274 (2018).
59. J. He, Y. en Du, Y. Bai, J. An, X. Cai, Y. Chen, P. Wang, X. Yang and Q. Feng, *Molecules*, **24**, 1 (2019).
60. H. I. Jaafar, A. M. A. Alsammerraei and H. H. Hamdan, *Iraqi J. Sci.*, **53**, 827 (2012).
61. P. Makuła, M. Pacia and W. Macyk, *J. Phys. Chem. Lett.*, **9**, 6814 (2018).
62. Hikmawati, A. H. Watoni, D. Wibowo, Maulidiyah and M. Nurdin, *IOP Conf. Ser. Mater. Sci. Eng.*, **267**, 012005 (2017).
63. L. G. Wade, *Organic chemistry*, Prentice Hall Upper Saddle River, NJ (1999).
64. B. Ayoubi-Feiz, M. H. Mashhadizadeh and M. Sheydaei, *Sep. Purif. Technol.*, **211**, 704 (2019).
65. M. Sheydaei, M. Karimi and V. Vatanpour, *J. Photochem. Photobiol. A: Chem.*, **384**, 112068 (2019).
66. G. Roselló-Márquez, R. M. Fernández-Domene, R. Sánchez-Tovar, M. Cifre-Herrando and J. García-Antón, *J. Environ. Chem. Eng.*, **9**, 105371 (2021).
67. D. Wibowo, M. Z. Muzakkar, S. K. M. Saad, F. Mustapa, M. Maulidiyah, M. Nurdin and A. A. Umar, *J. Photochem. Photobiol. A Chem.*, **398**, 112589 (2020).
68. M. Maulidiyah, I. B. P. Wijawan, D. Wibowo, A. Aladin, B. Hamzah and M. Nurdin, *IOP Conf. Ser. Mater. Sci. Eng.*, **367**, 012060 (2018).
69. M. Maulidiyah, D. Wibowo, H. Herlin, M. Andarini, R. Ruslan and M. Nurdin, *Asian J. Chem.*, **29**, 2504 (2017).
70. M. Z. Muzakkar, A. A. Umar, I. Ilham, Z. Saputra and L. Zulfikar, *J. Phys. Conf. Ser.*, **1242**, 1 (2019).